JCI The Journal of Clinical Investigation

Epicardial YAP/TAZ orchestrate an immunosuppressive response following myocardial infarction

Vimal Ramjee, Deqiang Li, Lauren J. Manderfield, Feiyan Liu, Kurt A. Engleka, Haig Aghajanian, Christopher B. Rodell, Wen Lu, Vivienne Ho, Tao Wang, Li Li, Anamika Singh, Dasan M. Cibi, Jason A. Burdick, Manvendra K. Singh, Rajan Jain, Jonathan A. Epstein

J Clin Invest. 2017;127(3):899-911. https://doi.org/10.1172/JCI88759.

Research Article **Cardiology** **Cell biology**

Ischemic heart disease resulting from myocardial infarction (MI) is the most prevalent form of heart disease in the United States. Post-MI cardiac remodeling is a multifaceted process that includes activation of fibroblasts and a complex immune response. T-regulatory cells (Tregs), a subset of $CD4^+$ T cells, have been shown to suppress the innate and adaptive immune response and limit deleterious remodeling following myocardial injury. However, the mechanisms by which injured myocardium recruits suppressive immune cells remain largely unknown. Here, we have shown a role for Hippo signaling in the epicardium in suppressing the post-infarct inflammatory response through recruitment of Tregs. Mice deficient in epicardial YAP and TAZ, two core Hippo pathway effectors, developed profound post-MI pericardial inflammation and myocardial fibrosis, resulting in cardiomyopathy and death. Mutant mice exhibited fewer suppressive Tregs in the injured myocardium and decreased expression of the gene encoding IFN-γ, a known Treg inducer. Furthermore, controlled local delivery of IFN-γ following MI rescued Treg infiltration into the injured myocardium of YAP/TAZ mutants and decreased fibrosis. Collectively, these results suggest that epicardial Hippo signaling plays a key role in adaptive immune regulation during the post-MI recovery phase.

Epicardial YAP/TAZ orchestrate an immunosuppressive response following myocardial infarction

Vimal Ramjee,[1,2,3,4] Deqiang Li,[1,2,3,4] Lauren J. Manderfield,[1,2,3,4] Feiyan Liu,[1,2,3,4] Kurt A. Engleka,[1,2,3,4] Haig Aghajanian,[1,2,3,4] Christopher B. Rodell,[5] Wen Lu,[6] Vivienne Ho,[1,2,3,4] Tao Wang,[1] Li Li,[1] Anamika Singh,[7] Dasan M. Cibi,[7] Jason A. Burdick,[5] Manvendra K. Singh,[7] Rajan Jain,[1,2,3,4] and Jonathan A. Epstein[1,2,3,4]

[1]Penn Cardiovascular Institute, [2]Department of Medicine, [3]Department of Cell and Developmental Biology, and [4]Institute for Regenerative Medicine, Perelman School of Medicine at the University of Pennsylvania, Philadelphia, Pennsylvania, USA. [5]Department of Bioengineering, University of Pennsylvania, Philadelphia, Pennsylvania, USA. [6]Department of Pathology and Laboratory Medicine, Perelman School of Medicine at the University of Pennsylvania, Philadelphia, Pennsylvania, USA. [7]Cardiovascular and Metabolic Disorders Program, Duke-NUS Medical School Singapore and National Heart Centre Singapore, Singapore.

Ischemic heart disease resulting from myocardial infarction (MI) is the most prevalent form of heart disease in the United States. Post-MI cardiac remodeling is a multifaceted process that includes activation of fibroblasts and a complex immune response. T-regulatory cells (Tregs), a subset of $CD4^+$ T cells, have been shown to suppress the innate and adaptive immune response and limit deleterious remodeling following myocardial injury. However, the mechanisms by which injured myocardium recruits suppressive immune cells remain largely unknown. Here, we have shown a role for Hippo signaling in the epicardium in suppressing the post-infarct inflammatory response through recruitment of Tregs. Mice deficient in epicardial YAP and TAZ, two core Hippo pathway effectors, developed profound post-MI pericardial inflammation and myocardial fibrosis, resulting in cardiomyopathy and death. Mutant mice exhibited fewer suppressive Tregs in the injured myocardium and decreased expression of the gene encoding IFN-γ, a known Treg inducer. Furthermore, controlled local delivery of IFN-γ following MI rescued Treg infiltration into the injured myocardium of YAP/TAZ mutants and decreased fibrosis. Collectively, these results suggest that epicardial Hippo signaling plays a key role in adaptive immune regulation during the post-MI recovery phase.

Introduction

Ineffective recovery after myocardial infarction (MI) remains the principal barrier to improving post-infarct outcomes and is associated with the development of heart failure in 1 of 4 patients (1, 2). Adverse remodeling of post-MI contractile myocardium into fibrotic tissue is a multifaceted phenomenon driven by a potent immune/inflammation cascade (3). Inflammation following myocardial injury invokes an exquisitely complex network of coordinated cytokine-, chemokine-, and leukocyte-driven responses resulting in myocardial fibrosis and chamber dilation. As a system not delimited to one pathogenic trigger, the immune network responds to a spectrum of cardiovascular diseases and is implicated in post-injury remodeling, the genesis of arrhythmias, and progression to heart failure (4, 5). Despite the crucial relationship between the maladaptive immune response and cardiovascular disease, there remains a paucity of investigation into this association.

Recently, a series of studies have demonstrated that the epicardium is activated following myocardial injury (6–10). The epicardium, the cellular layer adjacent to and surrounding the myocardium, was once considered a passive lining of the heart that provided a mechanical support to allow for optimal ventricular function (11, 12). During embryonic development, the epicardium can give rise to fibroblasts, smooth muscle cells, and endothelial cells within the heart (13, 14). Furthermore, a regenerative role for the epicardium after myocardial injury has been suggested over the past decade, wherein epicardial activation and reexpression of fetal gene programs following MI allows for repair of injured myocardium through intermediary epicardium-derived cells (EPDCs) (6, 10, 15–19), although this hypothesis is controversial (20). The activated epicardium after injury has also been implicated as a source of cytokines capable of modulating revascularization and repair of the damaged heart (21).

The Hippo signaling pathway, a highly conserved serine/threonine kinase cascade, has been shown to play a critical role in the heart through the function of 2 core effector proteins, yes-associated protein (YAP) and WW domain–containing transcription regulator 1 (WWTR1, referred to herein as TAZ) (22, 23). The upstream initiating factors that activate the Hippo pathway remain a topic of intense investigation, and recent studies have shown that GPCRs, as well as mechanical stimuli (i.e., cellular stretch), can engage this signaling cascade (24–26). In the post-MI setting, the sympathetic surge results in elevated levels of epinephrine, a known GPCR ligand that may play an important role in modulating Hippo. Fur-

Authorship note: V. Ramjee and D. Li contributed equally to this work.
Note regarding evaluation of this manuscript: Manuscripts authored by scientists associated with Duke University, The University of North Carolina at Chapel Hill, Duke-NUS, and the Sanford-Burnham Medical Research Institute are handled not by members of the editorial board but rather by the science editors, who consult with selected external editors and reviewers.
Conflict of interest: The authors have declared that no conflict of interest exists.
Submitted: May 25, 2016; **Accepted:** December 12, 2016.
Reference information: *J Clin Invest*. 2017;127(3):899–911.
https://doi.org/10.1172/JCI88759.

thermore, the eventual formation of a dense fibrotic scar from MI injury likely affects mechanical strain in the local cellular environment, thereby providing yet another cue to possibly engage Hippo signaling in the heart. Myocyte-specific deletion of *Yap* results in impaired cardiac regeneration in neonatal mice after left anterior descending (LAD) coronary artery ligation (27). Conversely, expression of a constitutively active form of YAP or inactivation of upstream Hippo kinases (mammalian STE20-like protein kinase 1/2 [MST1/2] or large tumor-suppressor homolog 1/2 [LATS1/2]) promotes cardiomyocyte proliferation after MI (27, 28). We have recently shown that YAP/TAZ play critical functions in the developing epicardium and that loss of YAP/TAZ function in embryonic epicardium affects myocardial development (29). Therefore, we hypothesized that epicardial Hippo signaling modulates myocardial remodeling after MI through paracrine mechanisms.

Over the past decade, there has been renewed interest in the role of the innate immune response in cardiovascular disease, although with little focus on the adaptive immune response after myocardial injury (30). Multiple cell types, including macrophages and T cells, play important roles in the adaptive immune response (31). Depletion of embryonic macrophages has been shown to abrogate the ability of the neonatal heart to regenerate (32). However, loss of macrophages during adult injury enhances scar formation in the adult (33, 34). Recently, T-regulatory cells (Tregs), a subset of $CD4^+$ T cells, have been shown to suppress the immune response following myocardial injury (35, 36). Tregs in various animal models have been shown to reduce the post-infarct scar size in the myocardium (36, 37), decrease immune infiltration in myocarditis (38), and suppress the development of atherosclerotic plaques (39). Furthermore, Tregs can potentiate recovery from skeletal muscle damage (40), autoimmune diseases (41), and infections (42). Loss of Tregs is thought to result in increased post-MI infarct size due to exacerbated cardiac inflammation, perdurance of proinflammatory macrophages, and delayed healing (35, 36). To date, the precise mechanism by which the injured myocardium recruits suppressive T cells remains unknown. This information is crucial to potentially refining the Treg response as part of any novel therapeutic strategy.

Multiple studies have demonstrated a critical role for Hippo signaling in controlling organ size and epithelial-to-mesenchymal transition. In this study, we demonstrate what we believe to be a novel role for YAP/TAZ signaling in post-MI epicardial derivatives through recruitment of Tregs to the injured myocardium. Loss of YAP/TAZ in epicardium results in a post-MI profibrotic response. This response is associated with a decrease in *IFN-g* (encoding IFN-γ), which is a direct transcriptional target of Hippo signaling. Using a bioengineered hydrogel, we partially rescue the mutant phenotype with local delivery of IFN-γ in the post-MI setting, thereby providing a translational framework for potential future therapeutic efforts.

Results

Epicardial Yap/Taz deletion produces fibrosis, cardiomyopathy, and death after MI. To elucidate the role of epicardial Hippo signaling in post-MI recovery, we inducibly deleted *Yap* and *Taz* in adult murine epicardium using the $Wt1^{CreERT2/+}$ allele, with tamoxifen injection 2 days preceding and 2 days following MI injury (Figure 1A), which resulted in efficient loss of epicardial YAP and TAZ protein expression (Figure 1B). Lineage tracing of epicardium after $Wt1^{CreERT2/+}$-mediated deletion of *Yap* and *Taz* revealed epicardial activation and expansion of epicardium-derived cells within the zone of injury produced by MI, but not by sham surgery (Figure 1, C and D). Thus, *Yap* and *Taz* are dispensable for at least some aspects of epicardial response to injury.

Two weeks after MI, the phenotype of the animals lacking epicardial *Yap/Taz* was striking. In every case (n = 5), deletion of *Yap/Taz* resulted in a thick, fibrous cap at the cardiac apex, as well as diffuse whitening along the pericardial surface, consistent with a hyperinflammatory response. This was never observed in control ($Yap^{fl/fl}$ $Taz^{fl/fl}$, tamoxifen-treated) mice after MI (n = 7) (Figure 2A). In each case, the cardiac apex of epicardial *Yap/Taz*–mutant animals was attached to and eroding into the soft tissue and bone structures of the anterior chest wall (Figure 2B). In contrast, control mice had localized fibrosis at the site of the coronary ligature and no adhesion to or erosion through the anterior chest wall (Figure 2B). Blanching during LAD coronary artery ligation, the presence of injury current on continuous telemetry during the operation, and fibrotic area quantified 2 days after MI were similar in control and mutant mice (n ≥3 per group, Supplemental Figure 1, A–C; supplemental material available online with this article; https://doi.org/10.1172/JCI88759DS1).

Serial images of coronary ligature–to-apex cross section specimens from controls showed localized fibrosis in the region of the infarct (Figure 3A). Strikingly, *Yap/Taz*-mutant specimens showed increased diffuse fibrosis throughout the left ventricular (LV) free wall (Figure 3A). Quantification of fibrotic scarring (as a percentage of the LV free wall cross-sectional area [CSA]) confirmed this observation (43.4% ± 3.2% $Yap^{fl/fl}$ $Taz^{fl/fl}$, n = 7 mice vs. 65.4% ± 8.2% $Wt1^{CreERT2/+}Yap^{fl/fl}$ $Taz^{fl/fl}$, n = 5 mice, $P < 0.05$) (Figure 3B). Neither sham-operated controls nor mutants exhibited substantial fibrosis (Supplemental Figure 1, D and E).

Further phenotyping revealed that epicardial *Yap/Taz*–mutant mice demonstrated disproportionate weight loss 1 week after MI, suggesting a failure to thrive (Figure 4A). Quantitative assessment of cardiac metrics with echocardiography after MI showed a significant decrease in LV stroke volume (SV) and cardiac output (CO) in mutant mice, indicative of a decrease in overall cardiac systolic function following loss of *Yap* and *Taz* (Figure 4, B–D). Other echocardiographic measurements were similar between the 2 groups, with the exception of the LV end-diastolic volume and LV systolic and diastolic lengths, which were also significantly reduced in the mutant mice (Supplemental Table 1). Baseline studies showed no significant difference in LV size or function between the 2 groups (Supplemental Figure 2). Kaplan-Meier survival analysis of 11 control and 12 mutant mice revealed a significantly higher mortality rate in the mutant group (Figure 4E).

Epicardial Yap/Taz deletion modulates post-MI cytokine response. To better understand the innate and adaptive immune effectors responsible for the exaggerated fibrotic response to MI in *Yap/Taz*-mutant mice, we assayed 84 immune genes by quantitative real-time PCR (qRT-PCR). Mutant and control mice were again treated with tamoxifen 2 days before and 2 days after MI injury, and RNA was isolated from the LV free wall, which included epicardium and EPDCs, 3 days after MI injury (n = 3 biological replicates for each genotype). Surprisingly, we found that only 2 of 84 assayed genes demonstrated significantly altered gene expression ($P < 0.05$).

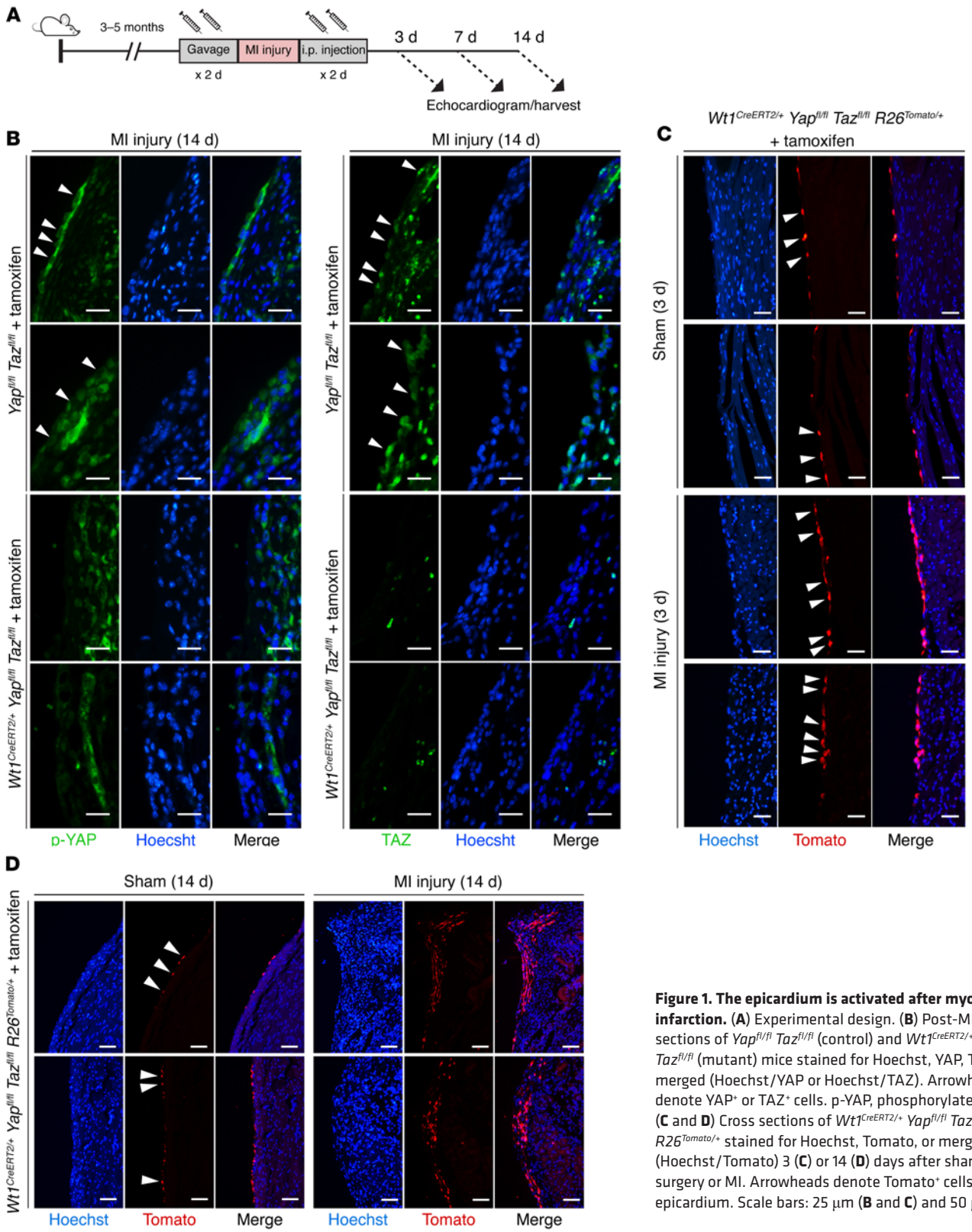

Figure 1. The epicardium is activated after myocardial infarction. (**A**) Experimental design. (**B**) Post-MI cross sections of *Yap*$^{fl/fl}$ *Taz*$^{fl/fl}$ (control) and *Wt1*$^{CreERT2/+}$ *Yap*$^{fl/fl}$ *Taz*$^{fl/fl}$ (mutant) mice stained for Hoechst, YAP, TAZ, or merged (Hoechst/YAP or Hoechst/TAZ). Arrowheads denote YAP$^+$ or TAZ$^+$ cells. p-YAP, phosphorylated YAP. (**C** and **D**) Cross sections of *Wt1*$^{CreERT2/+}$ *Yap*$^{fl/fl}$ *Taz*$^{fl/fl}$ *R26*$^{Tomato/+}$ stained for Hoechst, Tomato, or merged (Hoechst/Tomato) 3 (**C**) or 14 (**D**) days after sham surgery or MI. Arrowheads denote Tomato$^+$ cells in the epicardium. Scale bars: 25 μm (**B** and **C**) and 50 μm (**D**).

Furthermore, we found that IFN-β (*Ifnb*) levels were elevated in *Yap/Taz*-mutant hearts, while *IFN-g* expression was significantly downregulated (Figure 5, A–C). We observed less significant changes ($P < 0.10$) for 7 other cytokine genes: colony-stimulating factor 2 (*Csf2*), Toll-like receptor 4 (*Tlr4*), cluster of differentiation 80 (*Cd80*), C-C motif chemokine receptor 5 (*Ccr5*), C-C motif chemokine ligand 5 (*Ccl5*), cluster of differentiation 4 (*Cd4*), and *Tlr9*. No significant change was detected in the remaining 75 genes assayed. Immune arrays completed 14 days after MI ($n = 3$ biological replicates for each genotype, Supplemental Figure 3) suggested ongo-

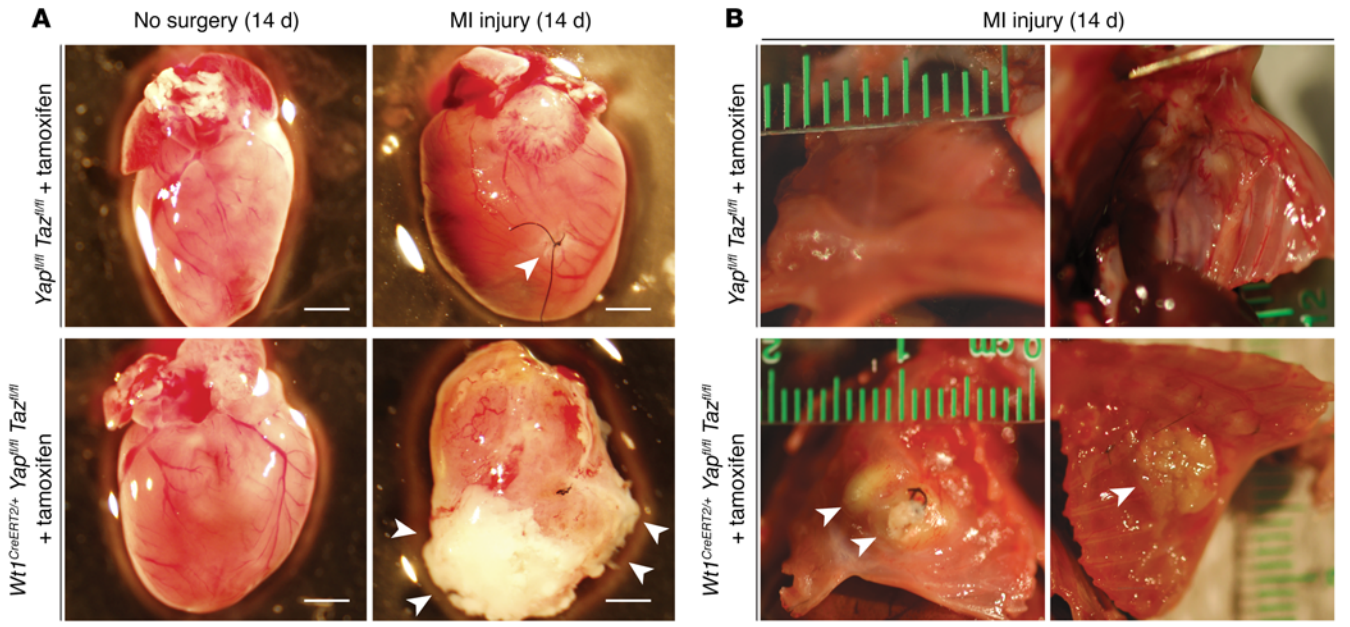

Figure 2. Deletion of epicardial YAP/TAZ results in profound pericardial inflammation and erosion of the heart through the chest wall. (**A**) Whole-mount bright-field images of representative *Yap*$^{fl/fl}$ *Taz*$^{fl/fl}$ (control) and *Wt1*$^{CreERT2/+}$ *Yap*$^{fl/fl}$ *Taz*$^{fl/fl}$ (mutant) hearts in the absence of surgery or following MI injury. Arrowheads indicate focal fibrosis at the site of the coronary ligature in control mice and a thick, fibrous cap covering the distal anterior LV wall and the entire cardiac apex in mutant mice. Scale bars: 2 mm. (**B**) Whole-mount bright-field images of representative *Yap*$^{fl/fl}$ *Taz*$^{fl/fl}$ (control) and *Wt1*$^{CreERT2/+}$ *Yap*$^{fl/fl}$ *Taz*$^{fl/fl}$ (mutant) chest walls following MI injury. Arrowheads denote erosion of the cardiac apex and anterior LV wall through the soft tissue and bone structures of the anterior chest wall in mutant mice.

ing inflammation in mutant hearts compared with that observed in control hearts. Interestingly, C-reactive protein (*Crp*), a robust inflammation biomarker, was increased by approximately 8-fold in mutant mice; however, this individual target did not reach statistical significance ($P = 0.105$, Supplemental Figure 3A).

Because YAP and TAZ are transcriptional coactivators, we focused on the most significantly downregulated gene in *Yap/Taz*-mutant hearts, i.e., *IFN-g*, at the peak of inflammation, 3 days after MI. It is well established that YAP and TAZ activate downstream genes by interacting with various DNA-binding cofactors including members of the TEA domain (TEAD) family of transcription factors (TEAD1–4), and analysis of the *IFNG* proximal promoter/enhancer revealed 17 potential TEAD-binding sites within 2 kb of the transcription start site. Luciferase reporter assays indicated that a 2-kb fragment of the *IFNG* promoter region was sufficient to induce 30- to 60-fold activation of reporter activity upon the introduction of YAP/TAZ as compared with controls (Figure 5D). The most proximal 400 bp, relative to the transcription start site, accounted for the majority of YAP/TAZ-dependent reporter activation (Figure 5D). YAP-mediated activation of the proximal 2-kb *IFNG* promoter was largely TEAD dependent, as evidenced by significant inhibition of YAP-dependent activation produced by the simultaneous introduction of a dominant-negative TEAD mutant (dnTEAD). This construct encodes a truncated protein that retains DNA-binding capacity but cannot recruit YAP or TAZ (Figure 5E) (43, 44). Chromatin immunoprecipitation(ChIP) assays confirmed that YAP could bind the *IFNG* proximal promoter, showing up to an 11-fold enrichment in YAP occupancy compared with a nearby region of the *IFNG* promoter (Figure 5F). Furthermore, ISH demonstrated expression of *IFN-g* in epicardial cells and their derivatives 3 days after MI injury, but not in those of sham-operated animals (Supplemental Figure 4). These findings support a direct role of injury in driving epicardium-activated cells to produce *IFN-g*.

Loss of cardiac IFN-g after MI results in defective Treg populations in the injured myocardium. Given that *IFN-g* is known to function as a Treg chemokine (45, 46), we examined Treg cell infiltration of the control and mutant hearts after injury. One week after MI, we noted a trend toward fewer Tregs in the LV free wall of mutant mice compared with LV free wall Treg numbers in control mice (17.0 ± 3.8 $CD3^+Foxp3^+$ cells in cross sections from 6 control sections vs. 9.7 ± 1.5 $CD3^+Foxp3^+$ in sections from 6 mutant sections, $P = 0.10$, mean ± SEM) (Figure 6A). Two weeks after MI, the difference was more striking: $CD3^+Foxp3^+$ Tregs were significantly more common in the LV free wall of control mice than in that of mutant mice (mean number of $CD3^+Foxp3^+$ cells per cross section: 48.1 ± 17.4 $CD3^+Foxp3^+$ cells in 5 control mice vs. 7.1 ± 1.4 cells in 6 mutant mice, $P < 0.05$, mean ± SEM) (Figure 6B). We found that the difference was most dramatic in the peri-infarct region, where clusters of $CD3^+Foxp3^+$ cells were easily identified in controls, while only rare isolated Tregs were identified in mutants. Importantly, the total pool of $CD4^+$ lymphocytes in the infarct region was similar between control and mutant mice (Supplemental Figure 5A). Thus, loss of *IFN-g* resulting from deletion of *Yap/Taz* in the epicardium is specifically associated with impaired Treg recruitment to injured myocardium and an exuberant fibrotic response. We also noted that the profibrotic response in mutant mice was accompanied by a significantly higher number of $F4/80^+$ macrophages in epicardial *Yap/Taz*–mutant mice after injury (Supplemental Figure 5B).

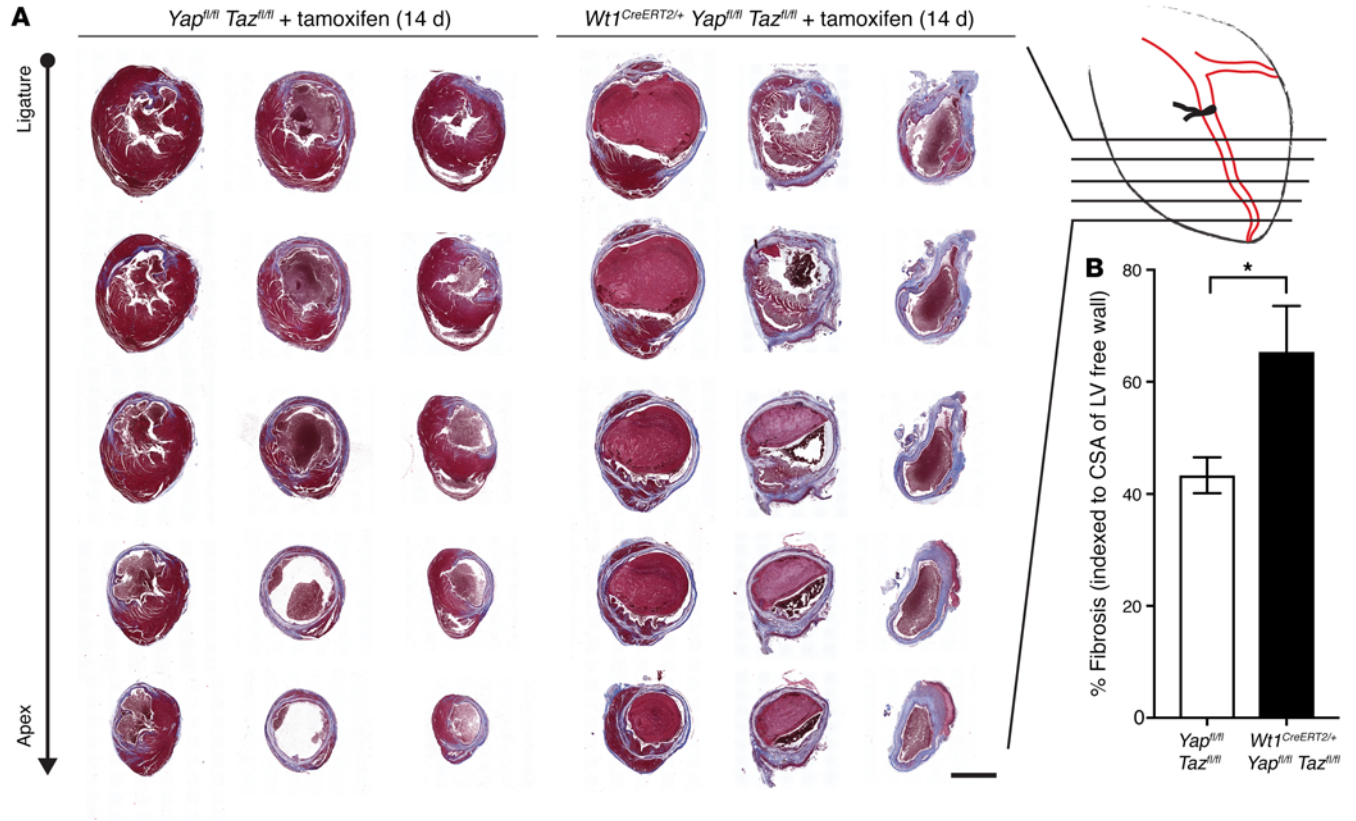

Figure 3. Deletion of epicardial *Yap/Taz* results in diffuse post-MI myocardial fibrosis. (**A**) Masson's trichrome staining of serial cross sections from the coronary ligature to the apex of the heart 14 days after MI in 3 representative control (*Yap*$^{fl/fl}$ *Taz*$^{fl/fl}$) and 3 representative mutant (*Wt1*$^{CreERT2/+}$ *Yap*$^{fl/fl}$ *Taz*$^{fl/fl}$) animals. Fibrotic tissue is stained blue. (**B**) Quantification of the proportion of fibrosis indexed to the total CSA of the myocardium in the LV free wall. There was a significantly greater amount of fibrosis in mutant hearts (65.4% ± 8.2%, n = 5 mice) compared with that in control hearts (43.4% ± 3.2%, n = 7 mice). *P < 0.05, by 2-tailed Student's t test. Data represent the mean ± SEM. Scale bar: 2 mm.

Next, we asked whether the post-MI hyperinflammatory phenotype correlates with changes in the systemic number of immune cells that are available to be recruited to the site of injury. First, we dissected and assayed immune cell populations of the spleen and mediastinal lymph nodes from mutant and control mice by flow cytometry to determine whether global or regional changes were present. We found no significant differences between control and mutant animals in the percentage of CD4$^+$ cells, CD8$^+$ cells, or Tregs in the spleen or mediastinal lymph nodes either 3 or 14 days after MI (Supplemental Figure 6, A and B). We observed a small but significant decrease in the percentage of B cells in the mediastinal lymph nodes of mutant mice 3 and 14 days after MI, although the absolute number of B cells was not significantly different (3 days after MI: controls, 2,362,525 ± 812,094 cells; mutants, 2,047,170 ± 1,587,636 cells; 14 days after MI: controls, 4,440,940 ± 2,987,237 cells; mutants, 3,137,575 ± 1,188,193 cells).

Local controlled delivery of IFN-γ rescues the mutant phenotype after MI injury. Given our collective findings implicating IFN-γ deficiency in the post-MI hyperinflammatory response in *Yap/Taz*-mutant mice, we hypothesized that IFN-γ treatment could partially rescue the excessive fibrosis noted in mutants by recruiting Tregs to the injured myocardium. Mutant mice (*Wt1*$^{CreERT2/+}$ *Yap*$^{fl/fl}$ *Taz*$^{fl/fl}$ *R26*$^{Tomato/+}$) underwent MI injury, and immediately following the procedure, hearts were either treated with an empty hyaluronic acid (HA) hydrogel or an IFN-γ–impregnated HA hydrogel (47). Mice treated with the control gel showed adhesion of the heart to the anterior chest wall and diffuse epicardial inflammation with friable tissue (Figure 7A, left). In contrast, mutants treated with IFN-γ–impregnated gel had no adhesion to the chest wall and had a clear epicardial surface on whole-mount bright-field examination (Figure 7A, right). We also noted a 34.4% relative reduction of myocardial fibrosis in the LV free wall of mice treated with IFN-γ (36.3% ± 3.5%, empty gel vs. 23.8% ± 3.6%, IFN-γ gel, P < 0.05, n = 4 mice in each cohort) (Figure 7B). Finally, immunohistochemical quantification revealed a 2-fold relative increase in CD3$^+$ Foxp3$^+$ Tregs within the infarcted LV free wall of IFN-γ–treated mutants (14.3 ± 5.4 CD3$^+$Foxp3$^+$ cells, empty gel vs. 30.3 ± 2.8 CD3$^+$Foxp3$^+$ cells, IFN-γ gel, P < 0.05, n = 4 mice in each cohort) (Figure 7, C and D). Collectively, these findings demonstrate that IFN-γ treatment is sufficient to locally increase Tregs and partially rescue the excessive fibrosis in mutants.

Discussion

Nearly 16 million adult Americans presently suffer from coronary heart disease (CHD), with an anticipated increase of 20% by 2030 (2). Approximately 25% of these adults develop heart failure after MI due to maladaptive remodeling of the myocardium (1, 2). Myocardial necrosis and cardiomyocyte apoptosis are the hallmarks of

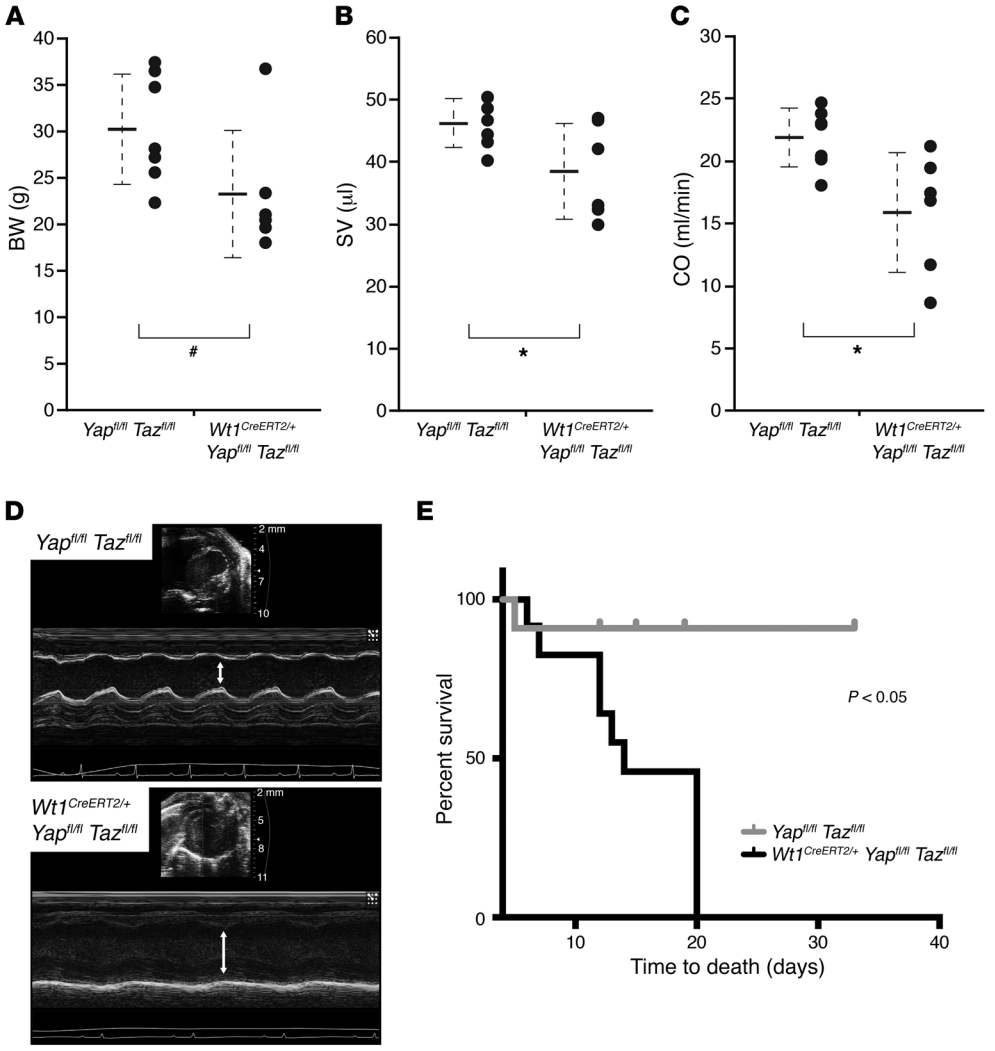

Figure 4. Loss of epicardial YAP/TAZ results in cardiomyopathy and increased mortality after MI injury. (**A**) BW measurement in $Yap^{fl/fl}$ $Taz^{fl/fl}$ (control, $n = 7$) and $Wt1^{CreERT2/+}$ $Yap^{fl/fl}$ $Taz^{fl/fl}$ (mutant, $n = 6$) animals 1 week after MI. (**B** and **C**) Echocardiographic examination of cardiac function including SV (**B**) and CO (**C**) in control ($n = 7$) and mutant mice ($n = 6$) 1 week after MI. Data represent the mean ± SD and are shown on the corresponding dot plots (**A**–**C**). $^{\#}P < 0.10$ and $^{*}P < 0.05$, by 2-tailed Student's t test. (**D**) M-mode echocardiographic evaluation confirmed decreased LV systolic function (white arrows: control, top panel; mutant, bottom panel) after MI injury. (**E**) Kaplan-Meier survival analysis of 11 control and 12 mutant mice after MI shows significantly greater mortality in the mutant group ($P < 0.05$, by log-rank test).

acute coronary syndromes, wherein a multitude of self-antigens actuate a profound immune response that allows for deleterious remodeling. Although a number of pharmacologic therapies targeting CHD have emerged over the past 2 decades, no immunomodulatory treatments are currently available to affect the post-MI inflammatory and fibrotic response.

Recent work has highlighted the emerging role that the epicardium plays in the developing heart as well as in the adult heart after myocardial injury (10, 17, 19, 48). Studies have shown that the epicardium becomes relatively quiescent after development but that there is robust reactivation of multiple fetal gene programs in the setting of myocardial injury (6, 8, 49). One factor implicated in this reactivation is thymosin β4 (Tβ4). Tβ4 is expressed in the myocardium only during development and provides a paracrine stimulus to the epicardium to promote cellular migration and differentiation (19). Tβ4 pretreatment, prior to injury, may activate epicardial cells, inducing them to adopt cardiac progenitor fates or to secrete salutary paracrine factors (10, 21, 50). The functional significance of epicardial activation after injury remained unclear until recently, with multiple groups demonstrating the release of paracrine factors from the epicardium and epicardial derivatives upon activation (7, 9, 18, 51, 52). There are both in vivo and in vitro data showing that the activated epicardium produces VEGFA and FGF2, factors that promote angiogenesis in the remodeling tissue (18). Throughout embryonic development, the epicardium stimulates myocardial proliferation through the secretion of mitogenic factors including FGF9/16/20 (53–55). Therefore, epicardial activation following MI injury in the adult heart may recapitulate developmental mechanisms to serve as a source of signaling molecules directing myocardial repair in the post-MI setting.

In the present study, we have expanded on these findings with a translational approach in a genetic murine model demonstrating epicardial activation that modulates an adaptive immune response through paracrine mechanisms. We describe an unexpected role of epicardial YAP/TAZ in recruiting a specific subset of suppressive $CD4^+$ Tregs to injured myocardium after MI. The brisk systemic cascade that ensues after injury, with the incursion of innate immune cells, is mediated at least in part by Tregs. These cells have emerged as critical homeostatic controllers to ensure that maladaptive inflammation is attenuated in a spectrum of disease states including myocardial injury from ischemia (35–40, 56, 57). Through pleiotropic effects, including release of suppressor cytokines, sequestration of proinflammatory cytokines, and direct cytotoxic effects on proinflammatory immune cells, Tregs are able

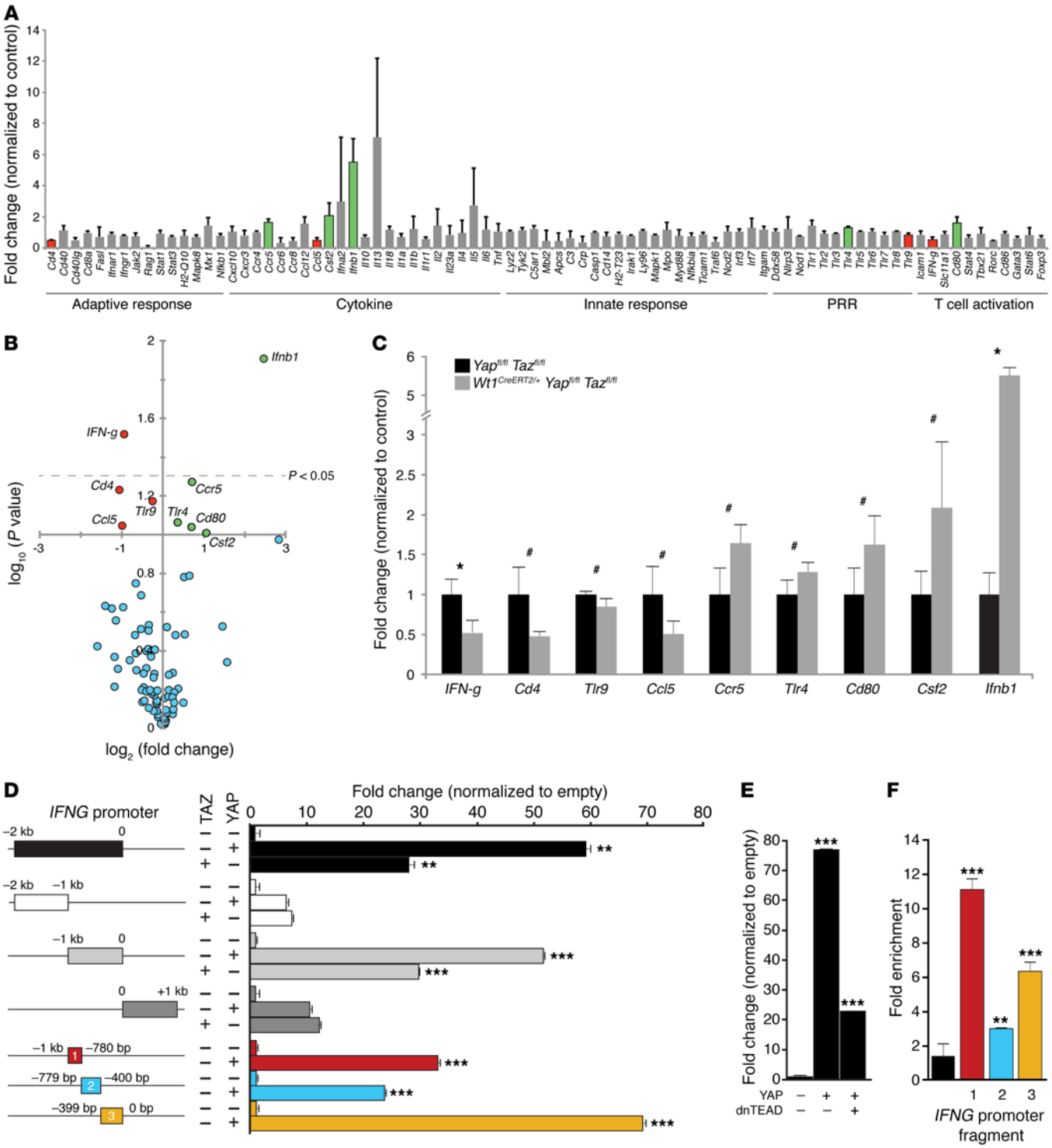

Figure 5. Epicardial YAP and TAZ directly modulate the immune target IFN-γ in the acute recovery phase after MI. (**A** and **B**) Bar graph and volcano plot of qRT-PCR immune arrays from microdissected LV free walls of control (*Yap*$^{fl/fl}$ *Taz*$^{fl/fl}$) and mutant (*Wt1*$^{CreERT2/+}$ *Yap*$^{fl/fl}$ *Taz*$^{fl/fl}$) animals 3 days after MI. Green bars/circles represent statistically significant upregulated genes, and red bars/circles represent significantly downregulated genes in mutant mice versus control mice ($n = 3$ in both groups, $P < 0.10$). (**B**) Circles above the dotted line have a P value of less than 0.05. Data for each gene were compared using a 2-tailed Student's t test. (**C**) Bar graph showing specific fold changes for up- and downregulated genes in the qRT-PCR immune arrays ($n = 3$ in both groups). (**D** and **E**) Luciferase reporter assays in HEK293T cells using various fragments of the *IFNG* promoter in the presence or absence of YAP, TAZ, or dnTEAD, as indicated. (**F**) YAP ChIP demonstrated significant YAP occupancy at the *IFNG* promoter (0 to –1 kb). $n = 3$ for all pairwise comparisons. Data in **A**–**D** represent the mean ± SD; data in **F** represent the mean ± SEM. $^{\#}P < 0.10$, $^{*}P < 0.05$, $^{**}P < 0.01$, and $^{***}P < 0.001$, by 2-tailed Student's t test.

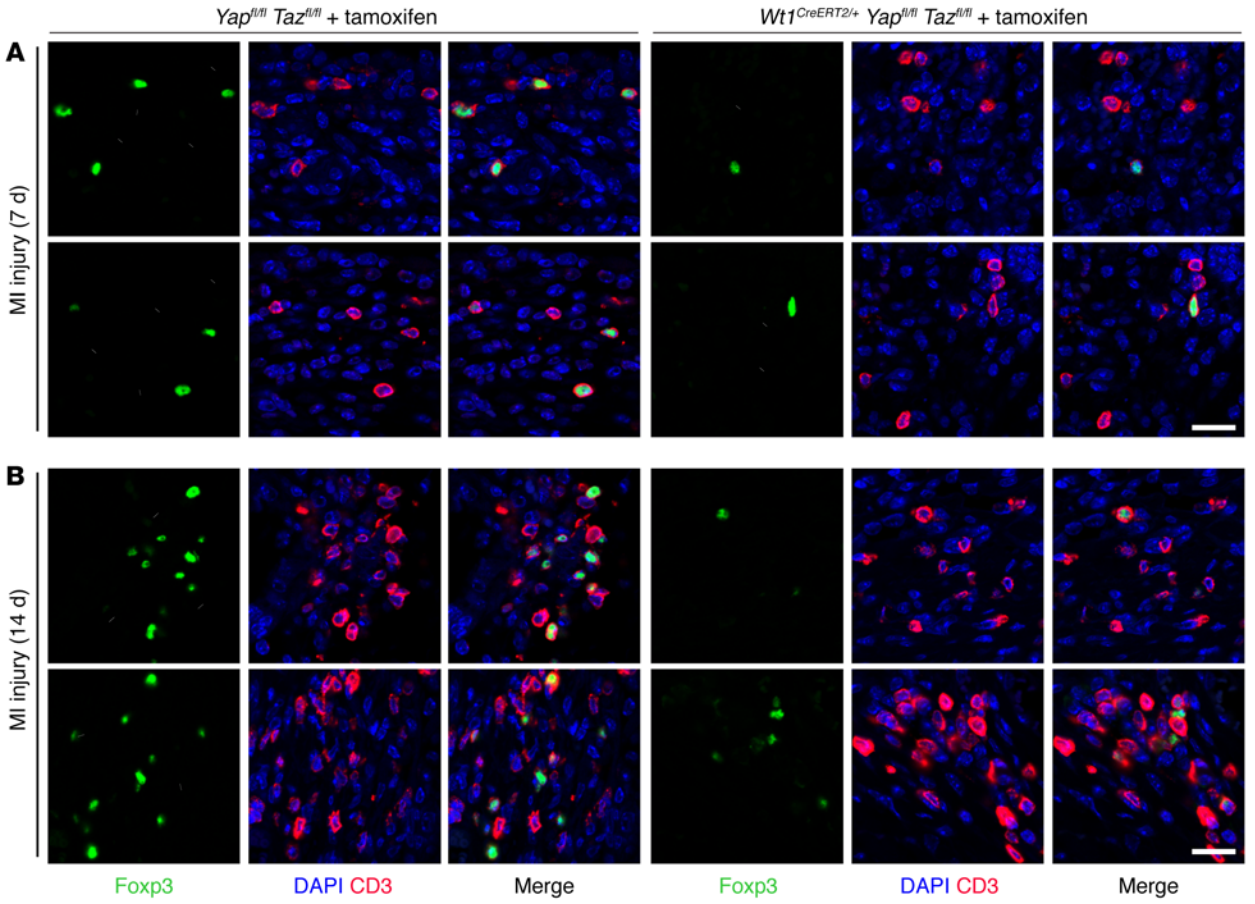

Figure 6. *Yap* and *Taz* deficiency results in impaired homing of Tregs to the injured heart. (**A** and **B**) Images of cross sections from *Yap*$^{fl/fl}$ *Taz*$^{fl/fl}$ and *Wt1*$^{CreERT2/+}$ *Yap*$^{fl/fl}$ *Taz*$^{fl/fl}$ animals 7 days (**A**) and 14 days (**B**) after MI, stained as indicated. See the Results and Methods sections regarding quantification. Scale bars: 20 μm.

to limit the amount of inflammation following tissue injury (58). Furthermore, by employing these collective suppressive mechanisms, Tregs are able to attenuate inflammation, despite being significantly less prevalent than are macrophages after MI injury (estimated 1 Treg for every 333 macrophages at 7 days after injury) (35). Interestingly, several studies have demonstrated an important role for IFN signaling in the activation and recruitment of Tregs to injured tissue (45, 46, 59, 60). IFN-γ has been shown in prior studies to affect multiple pathways, including suppression of fibrosis in chronic myocarditis by reducing profibrotic cytokine secretion (61), as well as mediation of basic FGF–induced (bFGF-induced) fibroblast migration via CXCL10 (62). Recently, however, Tregs have been shown to express the IFN-γ–specific receptors IFN-γR1 and IFN-γR2, thereby allowing a subset of these cells to be mediated directly by the chemokine IFN-γ (45). Additionally, the specific population of $CD4^+CD25^-$ T cells depends on IFN-γ to undergo conversion to Tregs in certain injury settings (46).

Our findings build on these studies by characterizing the process by which Tregs are recruited to injured myocardium. We demonstrate that the Hippo effectors YAP/TAZ function within epicardial derivatives to potently drive the production of the Treg chemokine IFN-γ after myocardial injury. Without epicardial YAP/TAZ, mutant mice have a significant deficiency of both IFN-γ and Tregs in the injured myocardium, and this deficiency is associated with myocardial fibrosis and increased mortality. We hypothesize that the increased mortality of the mutant mice likely reflects a combined burden of systolic dysfunction and diastolic dysfunction due to abundant cardiac scarring, though we cannot formally exclude arrhythmogenesis or progression of a restrictive/constrictive process as contributing factors. Restoration of IFN-γ levels via an ectopic hydrogel placed at the time of infarct in mutant animals partially rescued Treg infiltration into the myocardium and reduced fibrosis. The overall scar size was smaller in mice treated with empty hydrogel than that in untreated mice. We attribute this to well-established benefits inherent to the hydrogel itself, including a reduction in LV wall stress via a mechanical patch effect, as well as immunogenic alteration by HA (63–65). Our findings directly inform potential therapeutic efforts that may be targeted to post-MI recovery through immunomodulation. It will be interesting to determine whether other important clinical syndromes including pericarditis (66, 67), post-pericardiotomy syndrome (68), and Dressler syndrome (69), which share a hyperinflammatory pathophysiologic basis, may also benefit from enhanced Treg recruitment to the heart. Modulation of YAP/TAZ may be one method to regulate post-MI inflammation, but it will be important to more comprehensively understand the nonimmune roles of YAP/TAZ in the epicardium before conducting any human studies.

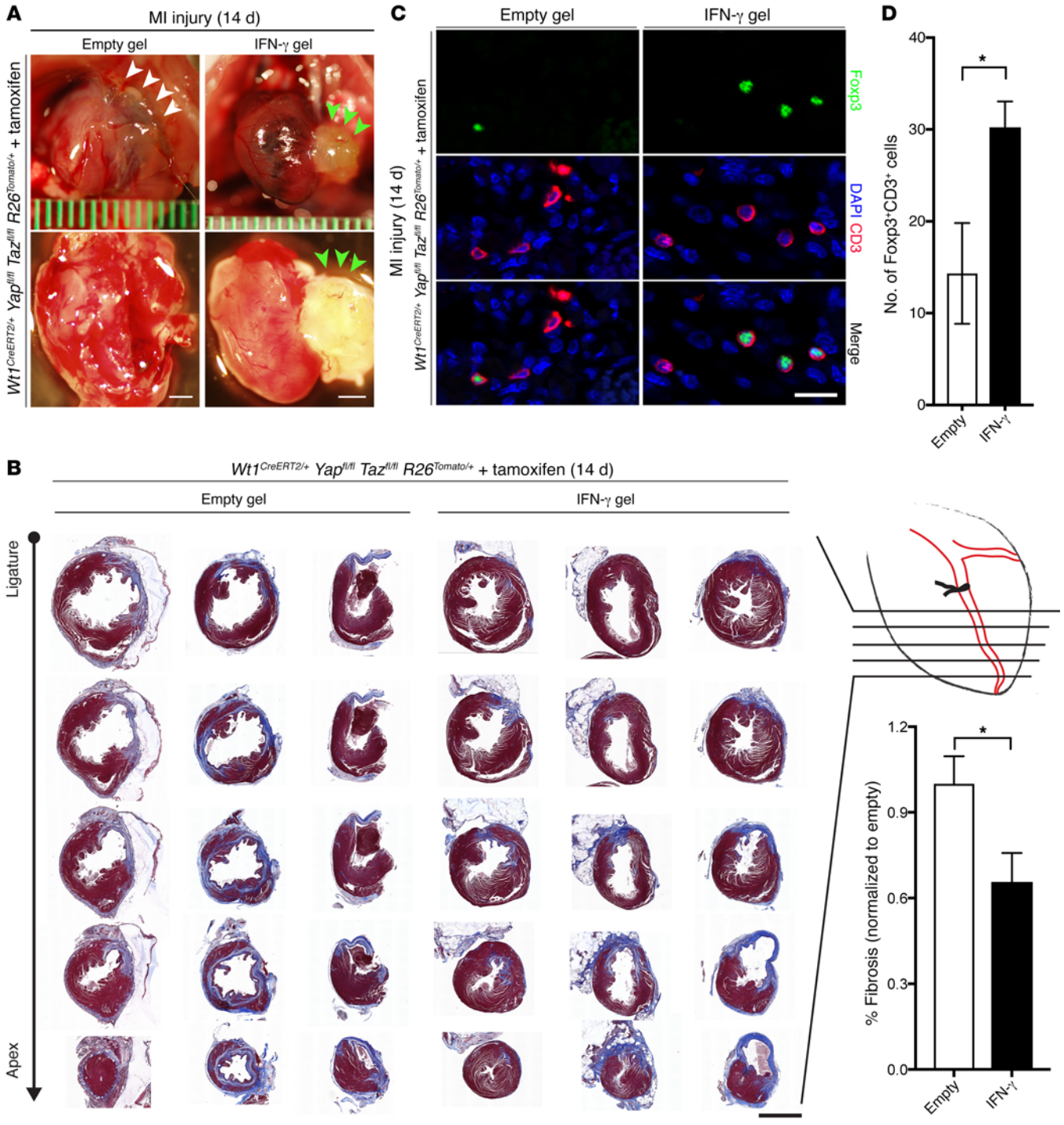

It has become clear that the crosstalk between the immune system and the heart involves multiple cell types communicating with each other over the course of the injury response to produce a scar. A recent report detailed how the epicardium instructs neutrophil infiltration (7). Overexpression of a dominant-negative form of the C/EBP transcription factor, specifically in the epicardium, prevents neutrophil recruitment to the damaged myocardium, resulting in improved ejection fraction and decreased scarring

(7). This beneficial response following loss of C/EBP function, in contrast to the deleterious results following loss of epicardial YAP/TAZ, highlights the importance of understanding the intricacies of paracrine signaling and the immune response in cardiac injury.

Our data linking YAP/TAZ to Treg recruitment provided a unique opportunity to characterize the role for epicardial activation in regulating the post-MI adaptive immune response. Of note, the loss of IFN-γ expression with deficient Treg recruitment to the injured myocardium likely has effects on other immune cell populations, including macrophages and neutrophils (58, 70, 71). In the present study, we found a greater number of F4/80$^+$ macrophages in the infarcted myocardium of epicardial YAP/TAZ–mutant mice 2 weeks after MI injury (Supplemental Figure 5B). This finding may be secondary to that of deficient Tregs in the injured myocardium (i.e., loss of the suppressive mechanism), or the result of alternative cytokine modulation. Future studies will be aimed at identifying cytokines that are misregulated within local niches in the injured myocardium. Though previous data have demonstrated that depletion of macrophages results in increased scar burden and a reduction in cardiac function (32–34), it is possible that secondary excessive infiltration of macrophages may also have deleterious effects. Following cardiac injury, 2 classes of macrophages, M1 and M2, are known to sequentially populate damaged myocardium (32, 72–74). After the first week of myocardial injury, M2 macrophages are predominant and promote fibrosis, possibly as a protective mechanism to prevent cardiac rupture (3, 75). Interestingly, embryonic cardiac macrophages have been found to be necessary for neonatal cardiac regeneration (32). In the future, it will be critical to decipher how macrophages and other immune cells functionally interact with Tregs and whether post-MI regeneration and remodeling can be beneficially modulated by targeting immune pathways.

Methods

Plasmids. The IFN-γ firefly-luciferase construct was generated by subcloning of specific IFN-γ–specific promoter regions (chr10:118439048-118441048, mm10) into pGL4.27 (Promega). The TEAD reporter, 8xGTIIC, murine *Yap*, murine *Taz*, and dominant-negative human *TEAD1* (*dnTEAD*) were all described previously (76).

Cell culture and luciferase assay. HEK293T cells were maintained at 37°C with 5% CO_2 in DMEM supplemented with 10% FBS, 1% penicillin, and 1% glutamate and streptomycin. All transfections were completed using FuGENE 6 (Roche). Luciferase experiments included 250 ng IFN-γ firefly-luciferase reporter constructs, 80 ng *Yap* or *Taz*, 80 ng *dnTEAD*, and 75 ng pGL2-Basic-*Renilla* luciferase (Promega). All transfections maintained an equal concentration of total DNA with transfection of pCMV-Sport6 empty vector (Invitrogen, Thermo Fisher Scientific). Cellular extracts were collected 48 hours after transfection and used in a dual-luciferase assay (Promega). Firefly luciferase activity was normalized to *Renilla* activity. All experiments were performed in biological triplicate experiments. Statistical differences between samples were analyzed using a Student's *t* test by comparing each value with empty vector control.

Histology, immunofluorescence, and ISH. Samples were harvested at the designated intervals after surgery, fixed overnight in 4% paraformaldehyde, and then dehydrated through an ethanol series. Samples were all paraffin embedded prior to sectioning. The following primary antibodies for immunofluorescence were used: anti-RFP (1:50; Rockland Immunochemicals Inc.; catalog 600-401-379); anti-Foxp3 (1:50; Ebioscience; catalog 14-5773-82); anti-WT1 (1:50; Santa Cruz Biotechnology Inc.; catalog SC192); anti-YAP (1:200; Cell Signaling Technology; catalog 4912S); anti-TAZ (1:100; Cell Signaling Technology; catalog 4883); anti-CD3 (1:200; Abcam; catalog 16669); anti-CD4 (1:100; Abcam; catalog 25475); and anti-F4/80 (1:50; BioLegend; catalog 122601). RNAscope ISH was completed using a mouse IFN-γ probe according to the protocols provided by the manufacturer (Advanced Cell Diagnostics Inc.; catalog 311391).

RNA isolation, complementary DNA synthesis, and qRT-PCR. RNA was isolated from LV free wall tissue 3 days after LAD coronary ligation. cDNA was synthesized using the RT^2 First Strand Kit (QIAGEN). qRT-PCR was performed in triplicate with RT^2 SYBR Green ROX Mastermix (QIAGEN) using RT^2 Profiler PCR Array plates for mouse innate and adaptive immune targets (QIAGEN; catalog 330231, PAMM-052ZC). Three biological replicate experiments were separately completed for each group.

ChIP. To examine YAP occupancy at the *IFN-g* promoter, chromatin was generated from three 100-mm dishes of HEK293T cells transfected with 800 ng of the full-length *IFN-g* -pGL4.27 reporter and 100 ng of murine WT YAP. Seventy-two hours after transfection, transfected cells were washed twice in cold PBS and cross-linked with 1% formaldehyde for 10 minutes at room temperature. Next, the reaction was quenched with the addition of 0.14 M glycine for 5 minutes at room temperature. Cells were collected in ice-cold PBS, centrifuged, and resuspended in SDS lysis buffer (10 mM Tris-HCl, pH 8.0, 10 mM NaCl, 3 mM $MgCl_2$, 1% NP-40, 1% SDS, 0.5% deoxycholic acid, and protease inhibitors). After a 10-minute incubation on ice, the chromatin was sheared using a BioRuptor sonicator (Diagenode). Chromatin (10 μg) was diluted in ChIP dilution buffer (16.7 mM Tris-HCl, pH 8.1, 167 mM NaCl, 0.01% SDS, and 1.1% Triton-X-100) and incubated overnight at 4°C with 0.5 μg anti-YAP rabbit polyclonal antibody (Cell Signaling Technology; catalog 4912S) or control rabbit IgG (Santa Cruz Biotechnology Inc.; catalog sc-2027). Protein G agarose beads were added to each reaction for 1 hour at 4°C. The agarose beads were washed once for 5 minutes with each of the following buffers: low-salt buffer, high-salt buffer, LiCl buffer, and TE buffer. Complexes were eluted in 200 μl elution buffer (1% SDS and 0.1 M $NaHCO_3$) at room temperature for 15 minutes. After the reversal of chromatin cross-linking, protein degradation, and DNA purification, samples were PCR amplified using primers for specific regions of the *IFN-g* promoter: fragment 1, forward: AACTAGGTACCAGACAGAGAAGGAAACTTTT; fragment 1, reverse: CTCAACTCGAGATTCCTCTGCCACTAAATAT; fragment 2, forward: GCGGCGGTACCTGAAACTCTTATTCATCATA; fragment 2, reverse: TATATCTCGAGCTTGGGCTTCTCAAACCAT; fragment 3, forward: ACTTAGGTACCAGTTTCCTTTTATTCAGCCG; fragment 3, reverse: ATATACTCGAGAGCCTGCACCTCTCT; negative control, forward: CATTAGGTACCTGCTGGGATTAAAGGTATGA; negative control, reverse: CCCGACTCGAGATACATAAGCATAAAGATTT.

Mice. All mice were maintained on a mixed genetic background. *Yap*$^{fl/+}$ (77) and *Taz*$^{fl/+}$ (27) alleles were genotyped as previously described. *Wt1*$^{CreERT2/+}$ mice (*Wt1*$^{tm2(cre/ERT2)Wtp}$/J) and *R26tdTomato* mice (B6.Cg-*Gt(ROSA)26Sortm14(CAG-tdTomato)Hze*/J) were obtained from The Jackson Laboratory (strain numbers 010912 and 007914, respectively) and genotyped as previously described (78, 79).

For fate-mapping and rescue experiments, both mutant and control groups had the genotype *Wt1*$^{CreERT2/+}$ *Yap*$^{fl/fl}$ *Taz*$^{fl/fl}$ *R26*$^{Tomato/+}$. For fate

mapping, both groups were induced with tamoxifen for 2 days prior to surgery, then control mice underwent sham surgery, while mutant mice underwent LAD ligation injury. For rescue experiments, all mice were induced with tamoxifen for 2 days prior to surgery and then underwent MI injury, followed by empty hydrogel treatment (control group) or IFN-γ gel treatment (treatment group). Following surgery, induction was completed with 2 additional days of tamoxifen treatment. For all other experiments, control mice had the genotype $Yap^{fl/fl}$ $Taz^{fl/fl}$, and mutant mice had the genotype $Wt1^{CreERT2/+}$ $Yap^{fl/fl}$ $Taz^{fl/fl}$.

MI surgery. MI surgery was performed as previously described (80, 81). Briefly, adult mice aged 3–5 months were induced with tamoxifen (100 μg/g BW) by gavage 2 days before MI injury. After an adequate depth of anesthesia by inhalation of isoflurane (1%–3%) was attained, the neck and chest regions were shaved and antiseptic solution applied. The mouse was fixed in a supine position with tape, and toe-pinch reflexes were checked throughout surgery to monitor the depth of anesthesia. The tongue was retracted, and a 20-gauge i.v. catheter was inserted into the trachea. The catheter was then connected to the mouse ventilator (MiniVent Type 845; Harvard Apparatus) via the Y-shaped connector. Mice were ventilated with a tidal volume of 0.25 to 0.35 ml and a respiratory rate of 100 to 110 breaths per minute. Next, a left thoracotomy was performed by separating the fourth and fifth intercostal spaces to expose the heart. The pericardium was opened and the heart visualized by gentle retraction on the rib cage. The left LAD coronary artery was permanently ligated to induce MI using an 8-0 silk suture. Complete occlusion of the LAD was visually confirmed by rapid myocardial blanching as well as ST-segment elevation on continuous electrocardiography. The sham procedure was performed in an identical manner, with the exception that the occluding ligature was not tied. Surgical incisions were closed in 2 layers with a 4-0 suture. Mice underwent the completion of tamoxifen induction with i.p. injections (100 μg/g BW) for 2 days after MI injury. Daily postoperative care was provided until the time of tissue harvesting. Animals that died from the surgical procedure were excluded from both groups in the survival analyses.

Echocardiography. For echocardiographic assessment, animal preparation was similar to that outlined in previous reports (81, 82). Briefly, adult mice were anesthetized with inhalation of isoflurane (2.5%–3.0%) using a nose cone. Mice were placed on a warm board in the supine position to keep the body temperature around 37°C. The chest hair was removed using hair removal gel cream. The limbs were taped onto the metal electrocardiographic leads. Warm acoustic gel was applied to the scan field as a coupling medium.

Using a VisualSonics Vevo 2100 system and a 30-MHz transducer, M-mode images and real-time 2D B-mode cine loops of short- and long-axis views of the LV were acquired for cardiac structure and function assessment. Transmitral inflow Doppler spectra and tissue Doppler were recorded in an apical 4-chamber view for diastolic function assessments. Echocardiographic images were downloaded and analyzed off-line using VevoLab software (VisualSonics Inc.). At least 3 beats were measured and averaged for the interpretation of each given measurement. A single observer blinded to the experimental conditions as well as the histology results performed all image analyses.

Immune cell flow cytometry. Mediastinal lymph nodes and spleens were collected from mice immediately after harvesting whole hearts. Lymph node tissue was homogenized between the frosted regions of 2 glass slides in the presence of media for each mouse. Splenic tissue was homogenized using a 10-ml syringe in the presence of media for each mouse. Large particulate cell debris was filtered out of each suspension through a 70-μm mesh and slow-speed centrifugation. Red blood cells in the homogenate were then lysed at room temperature with an rbc lysis buffer for 10 minutes and resuspended in media for cell counting.

Prior to staining with the antibody master mix, a small aliquot of the homogenized cell suspension was stained with trypan blue to count the total number of live wbc using a hemocytometer. Subsequently, each major group of immune cells was quantitated using data collected on a FACSCanto cytometer (BD Biosciences) and analyzed by FlowJo software (Tree Star), with the following antigenic definition for each cell type: %B cells = single, live, $CD19^+$; %CD4 = single, live, $CD4^+$; %CD8 = single, live, $CD8^+$; and %Treg = single, live, $CD4^+$, $CD25^+$, $Foxp3^+$. The absolute number of cells was defined as the percentage of cell populations for each group defined multiplied by the total number of cells quantitated.

The antibody reagents anti-CD25 (PC61) and anti-CD19 (1D3) were purchased from BD Pharmingen and anti-Foxp3 (FJK-16s), anti-CD4 (RM4-5), and anti-CD8 (53-6.7) from eBioscience. Cells were stained with antibodies against surface antigens at 4°C for 20 minutes in PBS. Intracellular Foxp3 staining was performed with the Foxp3 Staining Buffer Set (eBioscience) according to the manufacturer's protocol.

Quantification of cardiac Tregs. Sections from the coronary ligature to the cardiac apex for mutant and control mice were stained with CD3 and Foxp3, counterstained with a nuclear marker (DAPI), and examined under the microscope. The numbers of $CD3^+Foxp3^+$ cells were manually counted in the LV free wall region in each of 3 sections chosen at similar anatomic levels for each heart. Statistical differences between groups were evaluated with a Student's *t* test.

Fibrosis image analysis. We quantified the amount of post-MI myocardial fibrosis in mutant and control mice using a color segmentation method in ImageJ (NIH) that has been previously described (83). Briefly, serial sections from the coronary ligature to the cardiac apex in mutant and control mice after MI were stained for Masson's trichrome to mark fibrotic tissue. Five cross-sectional images for each heart were analyzed using a color threshold in ImageJ for blue myocardium only (scar tissue), followed by the total myocardium. Analysis was limited to the LV free wall. Statistical differences in the percentage of fibrosis were evaluated with a Student's *t* test.

Hydrogel drug delivery. We performed rescue experiments on $Wt1^{CreERT2/+}$ $Yap^{fl/fl}$ $Taz^{fl/fl}$ $R26^{Tomato/+}$ mice using an HA polymer modified by hydroxyethyl methacrylate (HEMA-HA, 20% modification) to render it photopolymerizable and hydrolytically degradable (64). Hydrogel precursor solutions (25 μl per animal) consisted of HEMA-HA (6.0% weight) dissolved in a photoinitiator solution, as previously described (47), and contained either 1 μg recombinant IFN-γ (485-MI/CF; R&D Systems) or no drug. Each mouse underwent MI injury, and the hydrogel depot was subsequently formed onto the epicardial surface by application of the prepared precursor solution using a 28-gauge needle through the thoracotomy. Continual curing lamp exposure (Elipar 2500; 3M) was used throughout the solution application, with subsequent continued exposure for 2 minutes to allow for completion of hydrogel polymerization.

Statistics. Two-tailed Student's *t* tests were used to evaluate differences between groups in all cases, except when comparing the Kaplan-Meier curves, for which a log-rank test was performed. All data represent the mean ± SD unless otherwise noted. A *P* value of less than 0.05 was considered statistically significant.

Study approval. All animal work was performed using protocols approved by the IACUC of the University of Pennsylvania.

Author contributions

VR designed and performed experiments, analyzed data, and wrote the manuscript. LJM oversaw portions of the project, provided reagents, analyzed data, and wrote the manuscript. DL, CBR, FL, MKS, KAE, VH, AS, DMC, and LL designed and performed experiments. DL, HA, RJ, TW, and WL performed experiments and edited the manuscript. JAB oversaw the hydrogel rescue portions of the project. JAE, RJ, and MKS oversaw the entire project, designed experiments, analyzed data, and wrote the manuscript.

Acknowledgments

We are grateful to Eric N. Olson (University of Texas Southwestern Medical Center) for providing *Yap*$^{fl/fl}$ *Taz*$^{fl/fl}$ mice and to members of the Epstein laboratory (especially Andrey Poleshko) for many helpful discussions and technical support. We would also like to thank Taku Kambayashi (Department of Pathology and Laboratory Medicine, University of Pennsylvania) for helpful technical support with immune cell analyses and Chris Highley (Department of Bioengineering, University of Pennsylvania) for technical support with hydrogel implantation. This work was supported by the Division of Cardiology of the University of Pennsylvania (grant T32, to VR); a Predoctoral Fellowship Award from the American Heart Association (to CBR); an Established Investigator Award from the American Heart Association (to JAB); the Burroughs Wellcome Fund (to RJ); the Singapore National Research Foundation (NRF-NRFF2016-01, to MKS); the Cotswold Foundation; the WW Smith Endowed Chair; and the NIH (U01 HL100405, to JAE, and K08 HL119553, to RJ).

Address correspondence to: Manvendra K. Singh, Duke-NUS Medical School, 8 College Road, Level 8-15, Singapore 169857. Phone: 65.66.013.098; E-mail: manvendra.singh@duke-nus.edu.sg. Or to: Rajan Jain, 09-102 Smilow Center for Translational Research, 3400 Civic Center Blvd., University of Pennsylvania, Philadelphia, PA 19104. Phone: 215.573.3011; E-mail: jainr@mail.med.upenn.edu. Or to: Jonathan A. Epstein, 602 PCAM South Expansion, 3400 Civic Center Blvd., Philadelphia, PA 19104. Phone: 215.573.9306; E-mail: epsteinj@upenn.edu.

VR's present address is: The Chattanooga Heart Institute, Chattanooga, Tennessee, USA.

LJM's present address is: GlaxoSmithKline, Collegeville, Pennsylvania, USA.

WL's present address is: Cleveland Clinic, Cleveland, Ohio, USA.

VH's present address is: Herspiegel Consulting, Yardley, Pennsylvania, USA.

1. Jhund PS, McMurray JJ. Heart failure after acute myocardial infarction: a lost battle in the war on heart failure? *Circulation*. 2008;118(20):2019–2021.
2. Mozaffarian D, et al. Heart disease and stroke statistics--2015 update: a report from the American Heart Association. *Circulation*. 2015;131(4):e29–e322.
3. Frangogiannis NG. Regulation of the inflammatory response in cardiac repair. *Circ Res*. 2012;110(1):159–173.
4. Marchant DJ, Boyd JH, Lin DC, Granville DJ, Garmaroudi FS, McManus BM. Inflammation in myocardial diseases. *Circ Res*. 2012;110(1):126–144.
5. Coggins M, Rosenzweig A. The fire within: cardiac inflammatory signaling in health and disease. *Circ Res*. 2012;110(1):116–125.
6. van Wijk B, Gunst QD, Moorman AF, van den Hoff MJ. Cardiac regeneration from activated epicardium. *PLoS ONE*. 2012;7(9):e44692.
7. Huang GN, et al. C/EBP transcription factors mediate epicardial activation during heart development and injury. *Science*. 2012;338(6114):1599–1603.
8. Wang J, Karra R, Dickson AL, Poss KD. Fibronectin is deposited by injury-activated epicardial cells and is necessary for zebrafish heart regeneration. *Dev Biol*. 2013;382(2):427–435.
9. Limana F, et al. Myocardial infarction induces embryonic reprogramming of epicardial c-kit(+) cells: role of the pericardial fluid. *J Mol Cell Cardiol*. 2010;48(4):609–618.
10. Smart N, et al. De novo cardiomyocytes from within the activated adult heart after injury. *Nature*. 2011;474(7353):640–644.
11. Watkins MW, LeWinter MM. Physiologic role of the normal pericardium. *Annu Rev Med*. 1993;44:171–180.
12. Beloucif S, Takata M, Shimada M, Robotham JL. Influence of pericardial constraint on atrioventricular interactions. *Am J Physiol*. 1992; 263(1 Pt 2):H125–H134.
13. Mikawa T, Fischman DA. Retroviral analysis of cardiac morphogenesis: discontinuous formation of coronary vessels. *Proc Natl Acad Sci USA*. 1992;89(20):9504–9508.
14. Mikawa T, Gourdie RG. Pericardial mesoderm generates a population of coronary smooth muscle cells migrating into the heart along with ingrowth of the epicardial organ. *Dev Biol*. 1996;174(2):221–232.
15. Masters M, Riley PR. The epicardium signals the way towards heart regeneration. *Stem Cell Res*. 2014;13(3 Pt B):683–692.
16. Riley PR. An epicardial floor plan for building and rebuilding the mammalian heart. *Curr Top Dev Biol*. 2012;100:233–251.
17. Singh MK, Epstein JA. Epicardium-derived cardiac mesenchymal stem cells: expanding the outer limit of heart repair. *Circ Res*. 2012;110(7):904–906.
18. Zhou B, et al. Adult mouse epicardium modulates myocardial injury by secreting paracrine factors. *J Clin Invest*. 2011;121(5):1894–1904.
19. Vieira JM, Riley PR. Epicardium-derived cells: a new source of regenerative capacity. *Heart*. 2011;97(1):15–19.
20. Christoffels VM, Grieskamp T, Norden J, Mommersteeg MT, Rudat C, Kispert A. Tbx18 and the fate of epicardial progenitors. *Nature*. 2009;458(7240):E8–E9.
21. Smart N, et al. Thymosin beta4 induces adult epicardial progenitor mobilization and neovascularization. *Nature*. 2007;445(7124):177–182.
22. Johnson R, Halder G. The two faces of Hippo: targeting the Hippo pathway for regenerative medicine and cancer treatment. *Nat Rev Drug Discov*. 2014;13(1):63–79.
23. Zhou Q, Li L, Zhao B, Guan KL. The hippo pathway in heart development, regeneration, and diseases. *Circ Res*. 2015;116(8):1431–1447.
24. Yu FX, et al. Regulation of the Hippo-YAP pathway by G-protein-coupled receptor signaling. *Cell*. 2012;150(4):780–791.
25. Codelia VA, Irvine KD. Hippo signaling goes long range. *Cell*. 2012;150(4):669–670.
26. Codelia VA, Sun G, Irvine KD. Regulation of YAP by mechanical strain through Jnk and Hippo signaling. *Curr Biol*. 2014;24(17):2012–2017.
27. Xin M, et al. Hippo pathway effector Yap promotes cardiac regeneration. *Proc Natl Acad Sci USA*. 2013;110(34):13839–13844.
28. Heallen T, et al. Hippo signaling impedes adult heart regeneration. *Development*. 2013;140(23):4683–4690.
29. Singh A, et al. Hippo signaling mediators Yap and Taz are required in the epicardium for coronary vasculature development. *Cell Rep*. 2016;15(7):1384–1393.
30. Mann DL. The emerging role of innate immunity in the heart and vascular system: for whom the cell tolls. *Circ Res*. 2011;108(9):1133–1145.
31. Epelman S, Liu PP, Mann DL. Role of innate and adaptive immune mechanisms in cardiac injury and repair. *Nat Rev Immunol*. 2015;15(2):117–129.
32. Aurora AB, et al. Macrophages are required for neonatal heart regeneration. *J Clin Invest*.

2014;124(3):1382–1392.
33. van Amerongen MJ, Harmsen MC, van Rooijen N, Petersen AH, van Luyn MJ. Macrophage depletion impairs wound healing and increases left ventricular remodeling after myocardial injury in mice. *Am J Pathol*. 2007;170(3):818–829.
34. Leblond AL, et al. Systemic and cardiac depletion of M2 macrophage through CSF-1R signaling inhibition alters cardiac function post myocardial infarction. *PLoS ONE*. 2015;10(9):e0137515.
35. Nahrendorf M, Swirski FK. Regulating repair: regulatory T cells in myocardial infarction. *Circ Res*. 2014;115(1):7–9.
36. Weirather J, et al. Foxp3+ CD4+ T cells improve healing after myocardial infarction by modulating monocyte/macrophage differentiation. *Circ Res*. 2014;115(1):55–67.
37. Hofmann U, et al. Activation of CD4+ T lymphocytes improves wound healing and survival after experimental myocardial infarction in mice. *Circulation*. 2012;125(13):1652–1663.
38. Shi Y, et al. Regulatory T cells protect mice against coxsackievirus-induced myocarditis through the transforming growth factor beta-coxsackie-adenovirus receptor pathway. *Circulation*. 2010;121(24):2624–2634.
39. Ait-Oufella H, et al. Natural regulatory T cells control the development of atherosclerosis in mice. *Nat Med*. 2006;12(2):178–180.
40. Burzyn D, et al. A special population of regulatory T cells potentiates muscle repair. *Cell*. 2013;155(6):1282–1295.
41. Carbone F, et al. Regulatory T cell proliferative potential is impaired in human autoimmune disease. *Nat Med*. 2014;20(1):69–74.
42. Belkaid Y. Regulatory T cells and infection: a dangerous necessity. *Nat Rev Immunol*. 2007;7(11):875–888.
43. Zhang H, et al. TEAD transcription factors mediate the function of TAZ in cell growth and epithelial-mesenchymal transition. *J Biol Chem*. 2009;284(20):13355–13362.
44. Zhao B, et al. TEAD mediates YAP-dependent gene induction and growth control. *Genes Dev*. 2008;22(14):1962–1971.
45. Hall AO, et al. The cytokines interleukin 27 and interferon-γ promote distinct Treg cell populations required to limit infection-induced pathology. *Immunity*. 2012;37(3):511–523.
46. Wang Z, et al. Role of IFN-gamma in induction of Foxp3 and conversion of $CD4^+$ $CD25^-$ T cells to $CD4^+$ Tregs. *J Clin Invest*. 2006;116(9):2434–2441.
47. Purcell BP, Elser JA, Mu A, Margulies KB, Burdick JA. Synergistic effects of SDF-1α chemokine and hyaluronic acid release from degradable hydrogels on directing bone marrow derived cell homing to the myocardium. *Biomaterials*. 2012;33(31):7849–7857.
48. Russell JL, Goetsch SC, Gaiano NR, Hill JA, Olson EN, Schneider JW. A dynamic notch injury response activates epicardium and contributes to fibrosis repair. *Circ Res*. 2011;108(1):51–59.
49. Braitsch CM, Kanisicak O, van Berlo JH, Molkentin JD, Yutzey KE. Differential expression of embryonic epicardial progenitor markers and localization of cardiac fibrosis in adult ischemic injury and hypertensive heart disease. *J Mol Cell Cardiol*. 2013;65:108–119.
50. Smart N, et al. Myocardial regeneration: expanding the repertoire of thymosin β4 in the ischemic heart. *Ann N Y Acad Sci*. 2012;1269:92–101.
51. Lepilina A, et al. A dynamic epicardial injury response supports progenitor cell activity during zebrafish heart regeneration. *Cell*. 2006;127(3):607–619.
52. González-Rosa JM, Martín V, Peralta M, Torres M, Mercader N. Extensive scar formation and regression during heart regeneration after cryoinjury in zebrafish. *Development*. 2011;138(9):1663–1674.
53. Sucov HM, Gu Y, Thomas S, Li P, Pashmforoush M. Epicardial control of myocardial proliferation and morphogenesis. *Pediatr Cardiol*. 2009;30(5):617–625.
54. Lavine KJ, et al. Endocardial and epicardial derived FGF signals regulate myocardial proliferation and differentiation in vivo. *Dev Cell*. 2005;8(1):85–95.
55. Lu SY, et al. FGF-16 is required for embryonic heart development. *Biochem Biophys Res Commun*. 2008;373(2):270–274.
56. Saxena A, et al. Regulatory T cells are recruited in the infarcted mouse myocardium and may modulate fibroblast phenotype and function. *Am J Physiol Heart Circ Physiol*. 2014; 307(8):H1233–H1242.
57. Xia N, et al. Activated regulatory T-cells attenuate myocardial ischaemia/reperfusion injury through a CD39-dependent mechanism. *Clin Sci*. 2015;128(10):679–693.
58. Sakaguchi S, Yamaguchi T, Nomura T, Ono M. Regulatory T cells and immune tolerance. *Cell*. 2008;133(5):775–787.
59. Nishikawa H, et al. IFN-gamma controls the generation/activation of CD4+ CD25+ regulatory T cells in antitumor immune response. *J Immunol*. 2005;175(7):4433–4440.
60. Namdar A, Nikbin B, Ghabaee M, Bayati A, Izad M. Effect of IFN-beta therapy on the frequency and function of CD4(+)CD25(+) regulatory T cells and Foxp3 gene expression in relapsing-remitting multiple sclerosis (RRMS): a preliminary study. *J Neuroimmunol*. 2010;218(1–2):120–124.
61. Fairweather D, et al. Interferon-gamma protects against chronic viral myocarditis by reducing mast cell degranulation, fibrosis, and the profibrotic cytokines transforming growth factor-beta 1, interleukin-1 beta, and interleukin-4 in the heart. *Am J Pathol*. 2004;165(6):1883–1894.
62. Bujak M, et al. Induction of the CXC chemokine interferon-gamma-inducible protein 10 regulates the reparative response following myocardial infarction. *Circ Res*. 2009;105(10):973–983.
63. Tous E, Purcell B, Ifkovits JL, Burdick JA. Injectable acellular hydrogels for cardiac repair. *J Cardiovasc Transl Res*. 2011;4(5):528–542.
64. Tous E, et al. Influence of injectable hyaluronic acid hydrogel degradation behavior on infarction-induced ventricular remodeling. *Biomacromolecules*. 2011;12(11):4127–4135.
65. Burdick JA, Prestwich GD. Hyaluronic acid hydrogels for biomedical applications. *Adv Mater Weinheim*. 2011;23(12):H41–H56.
66. Imazio M, Lazaros G, Brucato A, Gaita F. Recurrent pericarditis: new and emerging therapeutic options. *Nat Rev Cardiol*. 2016;13(2):99–105.
67. Lilly LS. Treatment of acute and recurrent idiopathic pericarditis. *Circulation*. 2013;127(16):1723–1726.
68. Alraies MC, Al Jaroudi W, Shabrang C, Yarmohammadi H, Klein AL, Tamarappoo BK. Clinical features associated with adverse events in patients with post-pericardiotomy syndrome following cardiac surgery. *Am J Cardiol*. 2014;114(9):1426–1430.
69. Spodick DH. Decreased recognition of the post-myocardial infarction (Dressler) syndrome in the postinfarct setting: does it masquerade as "idiopathic pericarditis" following silent infarcts? *Chest*. 2004;126(5):1410–1411.
70. Tang Q, Bluestone JA. The Foxp3+ regulatory T cell: a jack of all trades, master of regulation. *Nat Immunol*. 2008;9(3):239–244.
71. Grossman WJ, Verbsky JW, Barchet W, Colonna M, Atkinson JP, Ley TJ. Human T regulatory cells can use the perforin pathway to cause autologous target cell death. *Immunity*. 2004;21(4):589–601.
72. Pinto AR, Godwin JW, Rosenthal NA. Macrophages in cardiac homeostasis, injury responses and progenitor cell mobilisation. *Stem Cell Res*. 2014;13(3 Pt B):705–714.
73. Lavine KJ, et al. Distinct macrophage lineages contribute to disparate patterns of cardiac recovery and remodeling in the neonatal and adult heart. *Proc Natl Acad Sci USA*. 2014;111(45):16029–16034.
74. Nahrendorf M, et al. The healing myocardium sequentially mobilizes two monocyte subsets with divergent and complementary functions. *J Exp Med*. 2007;204(12):3037–3047.
75. Nahrendorf M, Swirski FK. Monocyte and macrophage heterogeneity in the heart. *Circ Res*. 2013;112(12):1624–1633.
76. Manderfield LJ, et al. Pax3 and hippo signaling coordinate melanocyte gene expression in neural crest. *Cell Rep*. 2014;9(5):1885–1895.
77. Xin M, et al. Regulation of insulin-like growth factor signaling by Yap governs cardiomyocyte proliferation and embryonic heart size. *Sci Signal*. 2011;4(196):ra70.
78. Zhou B, et al. Epicardial progenitors contribute to the cardiomyocyte lineage in the developing heart. *Nature*. 2008;454(7200):109–113.
79. Madisen L, et al. A robust and high-throughput Cre reporting and characterization system for the whole mouse brain. *Nat Neurosci*. 2010;13(1):133–140.
80. Tian Y, et al. A microRNA-Hippo pathway that promotes cardiomyocyte proliferation and cardiac regeneration in mice. *Sci Transl Med*. 2015;7(279):279ra38.
81. Yuan LJ, Wang T, Kahn ML, Ferrari VA. High-resolution echocardiographic assessment of infarct size and cardiac function in mice with myocardial infarction. *J Am Soc Echocardiogr*. 2011;24(2):219–226.
82. Yuan L, Wang T, Liu F, Cohen ED, Patel VV. An evaluation of transmitral and pulmonary venous Doppler indices for assessing murine left ventricular diastolic function. *J Am Soc Echocardiogr*. 2010;23(8):887–897.
83. Hartig SM. Basic image analysis and manipulation in ImageJ. *Curr Protoc Mol Biol*. 2013; Chapter 14:Unit14.15.